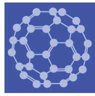 *nanomaterials*

MDPI

Article

The Effect of Annealing Ambience on the Material and Photodetector Characteristics of Sputtered $ZnGa_2O_4$ Films

Anoop Kumar Singh [1], Shiau-Yuan Huang [1], Po-Wei Chen [1], Jung-Lung Chiang [1] and Dong-Sing Wuu [1,2,3,*]

[1] Department of Materials Science and Engineering, National Chung Hsing University, Taichung 40227, Taiwan; anoop.scns@gmail.com (A.K.S.); ashin120606@gmail.com (S.-Y.H.); iversonc110307@gmail.com (P.-W.C.); cjunglung@gmail.com (J.-L.C.)

[2] Department of Applied Materials and Optoelectronic Engineering, National Chi Nan University, Nantou 54561, Taiwan

[3] Innovation and Development Center of Sustainable Agriculture, National Chung Hsing University, Taichung 40227, Taiwan

* Correspondence: dsw@ncnu.edu.tw or dsw@nchu.edu.tw

Abstract: Spinel $ZnGa_2O_4$ films were grown on c-plane sapphire substrates at the substrate temperature of 400 °C by radio-frequency magnetron sputtering. Post thermal annealing was employed at the annealing temperature of 700 °C in order to enhance their crystal quality. The effect of thermal annealing on the microstructural and optoelectronic properties of $ZnGa_2O_4$ films was systematically investigated in various ambiences, such as air, nitrogen, and oxygen. The X-ray diffraction patterns of annealed $ZnGa_2O_4$ films showed the crystalline structure to have (111) crystallographic planes. Transmission electron micrographs verified that $ZnGa_2O_4$ film annealed under air ambience possesses a quasi-single-crystalline structure. This $ZnGa_2O_4$ film annealed under air ambience exhibited a smooth surface, an excellent average transmittance above 82% in the visible region, and a wide bandgap of 5.05 eV. The oxygen vacancies under different annealing ambiences were revealed a substantial impact on the material and photodetector characteristics by X-ray photoelectron spectrum investigations. $ZnGa_2O_4$ film exhibits optimal performance as a metal-semiconductor-metal photodetector when annealed under air ambience. Under these conditions, $ZnGa_2O_4$ film exhibits a higher photo/dark current ratio of ~10^4 order, as well as a high responsivity of 2.53 A/W at the bias of 5 V under an incident optical light of 240 nm. These results demonstrate that quasi-single-crystalline $ZnGa_2O_4$ films have significant potential in deep-ultraviolet applications.

Keywords: $ZnGa_2O_4$; annealing ambience; wide bandgap; metal-semiconductor-metal photodetector; responsivity

Citation: Singh, A.K.; Huang, S.-Y.; Chen, P.-W.; Chiang, J.-L.; Wuu, D.-S. The Effect of Annealing Ambience on the Material and Photodetector Characteristics of Sputtered $ZnGa_2O_4$ Films. *Nanomaterials* **2021**, *11*, 2316. https://doi.org/10.3390/nano11092316

Academic Editor: Antonio Di Bartolomeo

Received: 17 July 2021
Accepted: 31 August 2021
Published: 6 September 2021

Publisher's Note: MDPI stays neutral with regard to jurisdictional claims in published maps and institutional affiliations.

Copyright: © 2021 by the authors. Licensee MDPI, Basel, Switzerland. This article is an open access article distributed under the terms and conditions of the Creative Commons Attribution (CC BY) license (https://creativecommons.org/licenses/by/4.0/).

1. Introduction

Deep-ultraviolet photodetectors (DUV PDs) based on $ZnGa_2O_4$ films are of substantial interest due to their prospective applications in flame monitoring, missile threat detection, ozone hole monitoring, engine control, optical communication, aerospace, and lithography alignment [1–4]. The high electrical conductivity and high electrochemical activities of $ZnGa_2O_4$ make it suitable for use as an anode material in rechargeable batteries [5]. $ZnGa_2O_4$ is a well-known phosphor material due to its intrinsic blue emission characteristics, which may be shifted to other emission wavelengths by doping metal ions or surface defects. It also exhibits a variety of functional features that can be applied to optoelectronic devices [6,7]. $ZnGa_2O_4$ possesses a wide bandgap in the region of 4.4–5.2 eV [8,9]. Its inherent chemical and thermal characteristics in a harsh environment along with high breakdown voltage make $ZnGa_2O_4$ a potential candidate for high-voltage devices, such as transistors and MOSFETs [10]. Wide bandgap semiconductors improve the efficiency of power-conversion stages, and they may be utilized instead of silicon in the production of voltage converters, power MOSFETs, and high-efficiency Schottky diodes. These can

then be employed in electric and hybrid cars [11]. Recently, Chi et al. and Chikoidze et al. demonstrated the p-type $ZnGa_2O_4$ semiconductor (5 eV), which could pave the way for bipolar oxide energy electronics by reducing switching and conversion losses. This is due to $ZnGa_2O_4$'s combination of the required qualities for sustaining large electrical fields in p-n junctions in the off-state, together with low losses in the on-state [12,13]. $ZnGa_2O_4$ possesses the cubic symmetric spinel structure with the space group of $Fd\bar{3}m$, where Zn^{2+} cations occupy tetrahedral sites and Ga^{3+} cations occupy octahedral sites with oxygen atoms in close-packed cubic structures [11,14].

There are other wide bandgap semiconductors such as β-Ga_2O_3 and $(Al_xGa_{1-x})_2O_3$, but these require high growth temperatures as well as high post-thermal annealing temperatures in order to create high-quality epitaxial films to employ in DUV spectral selection. Besides this, its anisotropic structural, optical, thermal, and mechanical characteristics including easy cleaving are the other drawbacks associated with β-Ga_2O_3. These drawbacks can be overcome using spinel $ZnGa_2O_4$, which offers a higher electrical conductivity, an isotropic cubic structure, distinguishable Zn and Ga cation sites, and a stable phase [15]. $ZnGa_2O_4$ is found to be suitable for use as the active layer in the fabrication of DUV PDs due to its insensitivity to light above the wavelength of 280 nm. Optoelectronic devices fabricated with one-dimensional nanostructures, such as nanotubes, nanowires, and nanocrystals, can achieve a high photoelectric conversion efficiency. However, in practice their stability and repeatability are still major concerns [16–18]. Hence, the development of $ZnGa_2O_4$ film-based PDs is essential. $ZnGa_2O_4$ films have been reported earlier by several research groups using radio-frequency (RF) magnetron sputtering [19,20], pulsed laser deposition [21], metal-organic chemical vapor deposition (MOCVD) [22], and mist-CVD [23]. Among these, RF magnetron sputtering is a cost-effective and dependable technology that is extensively utilized by industrial processes to build commercial optoelectronic devices. This is due to its ability to deposit films with a high purity, excellent compactness, repeatability, and homogeneity across a large area in less time than that taken by other technologies.

In this study, RF magnetron sputtering is used for depositing $ZnGa_2O_4$ films. The microstructural and optoelectronic characteristics of $ZnGa_2O_4$ films have been systematically investigated using an X-ray diffractometer, transmission electron microscope, atomic force microscope, field-emission scanning electron microscope, N&K analyzer, Keithley semiconductor parameter analyzer, and deuterium lamp with an Omni spectrometer. To date, the ambient effects of these thermal annealing processes have not been explored when assessing the material and photodetector characteristics of $ZnGa_2O_4$ films on sapphire substrates using RF magnetron sputtering.

2. Materials and Methods

$ZnGa_2O_4$ films (200 nm thickness) were deposited on 2-inch c-plane sapphire (0001) substrates using RF magnetron sputtering (model: SP-203, LHUHV, Hsinchu, Taiwan). The 3-inch ceramic target of $ZnGa_2O_4$, which had a purity of 99.99% (with a 50/50 ratio of ZnO/Ga_2O_3), was taken into consideration. The substrate was cleaned with acetone, isopropyl alcohol, and distilled water separately. It was then blown-dried with nitrogen gas before being introduced into the deposition chamber. When the base pressure had reached 1×10^{-6} Torr, the deposition of films was performed at the working pressure of 5×10^{-3} Torr and the substrate temperature of 400 °C. The rotation of the sample stage was maintained at 10 rpm to achieve a uniform thickness. The flow rate of argon gas was maintained at 10 sccm. Prior to sputtering, the target was pre-sputtered for 10 min by covering the target of the shutter in order to remove impurities on the surface of the $ZnGa_2O_4$. After this, the plasma was ignited by directing 100 W of RF power on the ceramic $ZnGa_2O_4$ target. As-deposited films were thermally annealed at a temperature of 700 °C using rapid thermal annealing (RTA, RTP-T41, Premtek International Inc., Hsinchu, Taiwan) for 1 min under air, nitrogen, and oxygen ambiences.

The thickness of the films was determined by an α-step profile analyzer. The crystallinity of the films was measured using a X-ray diffractometer (HR-XRD, X'Pert Pro MRD, PANanalytical, Almelo, Netherland). An N&K analyzer (model: 1280, n&k Technologies, San Jose, CA, USA) was used in this investigation to measure the transmittance of the $ZnGa_2O_4$ films. The optical bandgap of the films was extracted through Tauc plot. The surface morphology was determined using a field emission scanning electron microscope (FESEM, JSM-6700F, JEOL, Tokyo, Japan). The root-mean-square (RMS) surface roughness of the $ZnGa_2O_4$ films was measured using an atomic force microscope (AFM, Dimension 5000, Bruker, Santa Clara, CA, USA). The nanostructure and crystal orientations of the $ZnGa_2O_4$ films were studied using a transmission electron microscope (JEM-2100F, JEOL, Tokyo, Japan). The chemical states of the films were characterized by X-ray photoelectron spectroscopy (XPS, PHI 5000 Versa Probe, ULVAC-PHI, Kanagawa, Japan). The X-ray source for XPS was the monochromatized AlKα source (1486 eV). The X-ray beam size and takeoff angle were 100 μm and 45°, respectively. The pass energy was 58.7 eV. High-resolution scans were obtained by averaging 50 scans for O 1s peak in this investigation. Surface charging was minimized by an electron flood gun operated at 3 eV.

The metal-semiconductor-metal photodetector was fabricated with the interdigitated metal Ti/Au (with a thickness of 40/60 nm) Schottky contacts with the help of an electron-beam evaporator. These contacts were specified by photolithography and lift-off techniques. The active areas of the PDs were 1.05×1.05 mm^2, whereas the length, width, and spacing for the interdigital electrodes were specified as 950, 50, and 50 μm, respectively. The current–voltage characteristics were measured via a Keysight/Agilent semiconductor parameter analyzer (4155B, Hewlett-Packard Company, Englewood, CO, USA). A 30 W deuterium lamp was associated with the spectrometer (Omni-λ3029i, Zolix, Beijing, China) as the light source in the wavelength region of 200–360 nm, which helped us in the measurement of the spectral response of $ZnGa_2O_4$ PDs at the bias of 5 V.

3. Results and Discussion

Figure 1 shows the X-ray diffraction patterns of as-deposited and annealed $ZnGa_2O_4$ films under different annealing ambiences. As-deposited $ZnGa_2O_4$ film exhibited weak Bragg reflections for the (111), (222), and (511) planes, which corresponds to the spinel-cubic $ZnGa_2O_4$ (JCPDS card no-381240). The crystallinity of the as-deposited $ZnGa_2O_4$ film improved after thermal annealing under different ambiences. The thermal annealing of $ZnGa_2O_4$ films under air and nitrogen ambience dramatically increased the intensity of the (111), (222), and (511) planes, indicating that these films had a high crystallinity. In contrast, $ZnGa_2O_4$ film annealed under oxygen ambience had a low crystallinity, implying that this as-deposited film became oxidized after thermal annealing under an oxygen atmosphere. This shows that annealing in oxygen ambience can fulfill the oxygen vacancies in the $ZnGa_2O_4$ film, which leads to its oxidation and thus slight degradation in its crystallinity.

Figure 2a–h shows the AFM and SEM micrographs of as-deposited and annealed $ZnGa_2O_4$ films under different annealing ambiences. The RMS surface roughness of the as-deposited $ZnGa_2O_4$ film was 1.49 nm, whereas the RMS surface roughness of the annealed $ZnGa_2O_4$ film under air, nitrogen, and oxygen ambience was 1.37, 1.40, and 1.63 nm, respectively. This indicates that the $ZnGa_2O_4$ film annealed under air and nitrogen ambience had a smooth surface, which is beneficial for PDs. A smooth surface leads to a lower surface area, which results in low surface density states for the $ZnGa_2O_4$ film. The RMS surface roughness was found to be relatively larger after annealing under oxygen ambience, which could be due to the large amount of oxygen diffused by the adsorption of oxygen in the $ZnGa_2O_4$ film [24]. The SEM micrographs of the as-deposited $ZnGa_2O_4$ film revealed the columnar structure and irregular arrangement of grains with a rough surface, which were found to be dense and smooth after annealing under air and nitrogen ambiences with the presence of some nano-voids. It is well-known that high-temperature annealing reduces the surface energy between grains, which increases grain growth and reduces surface roughness due to the coalescence of small grains [25,26]. $ZnGa_2O_4$ film annealed under oxygen ambience was

found to be oxidized due to the absorption of oxygen in the film, which possesses a dense and highly rough surface with fewer nano-voids than other films [24]. These SEM results were found to be in accordance with the AFM and XRD results.

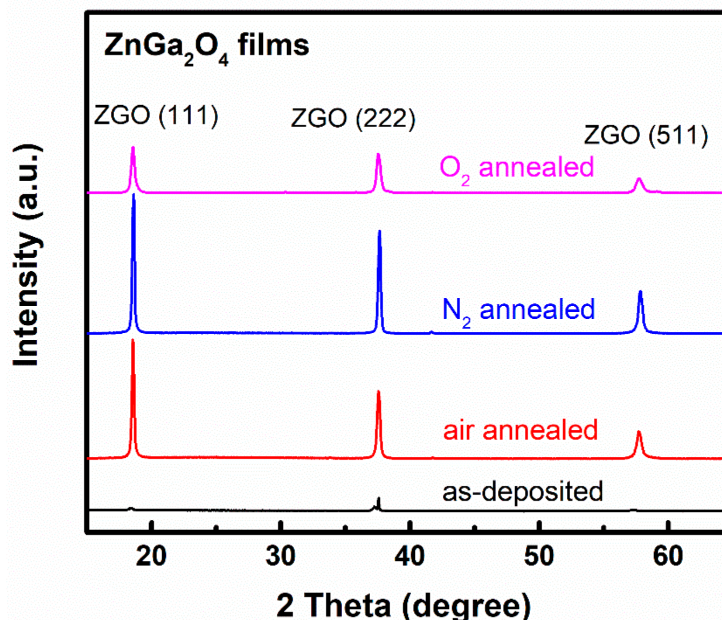

Figure 1. X-ray diffraction patterns of $ZnGa_2O_4$ (ZGO) films under different annealing ambiences.

Figure 3 depicts the cross-sectional and high-resolution transmission electron micrographs (HRTEM) of as-deposited and annealed $ZnGa_2O_4$ film under air ambience. The cross-sectional TEM micrograph of as-deposited $ZnGa_2O_4$ film is shown in Figure 3a, while region I and region II of this film are explored in Figure 3b,c, respectively. This as-deposited $ZnGa_2O_4$ film demonstrated columnar grains near the substrate region and possessed the amorphous, ZnO (100), Ga_2O_3 (201), and $ZnGa_2O_4$ (111) phases. These phases are evident in this film, as it was deposited at a substrate temperature of 400 °C. The d-spacing of ~2.83, 3.70, and 4.83 Å (compatible with 4.80 Å) was measured, which corresponded to the ZnO (111), Ga_2O_3(201), and $ZnGa_2O_4$ (111) phases, respectively. The rapid thermal annealing was performed at the temperature of 700 °C for 1 min under air ambience to improve the crystallinity of this film. The oxygen present in the air ambience during thermal annealing played a significant role in eliminating the intrinsic defects, such as amorphous regions and oxygen vacancies in the films. A cross-sectional TEM micrograph of the annealed $ZnGa_2O_4$ film under air ambience is shown in Figure 3d, and its region I and region II are explored in Figure 3e,f, respectively. These regions (I and II) of the annealed $ZnGa_2O_4$ film demonstrated that rapid thermal annealing under air ambience suppressed the amorphous and Ga_2O_3 phases by the local bond rearrangement at the interface between the amorphous phase and the crystalline phase, and achieved a quasi-single-crystalline $ZnGa_2O_4$ structure, as shown in Figure 3e,f.

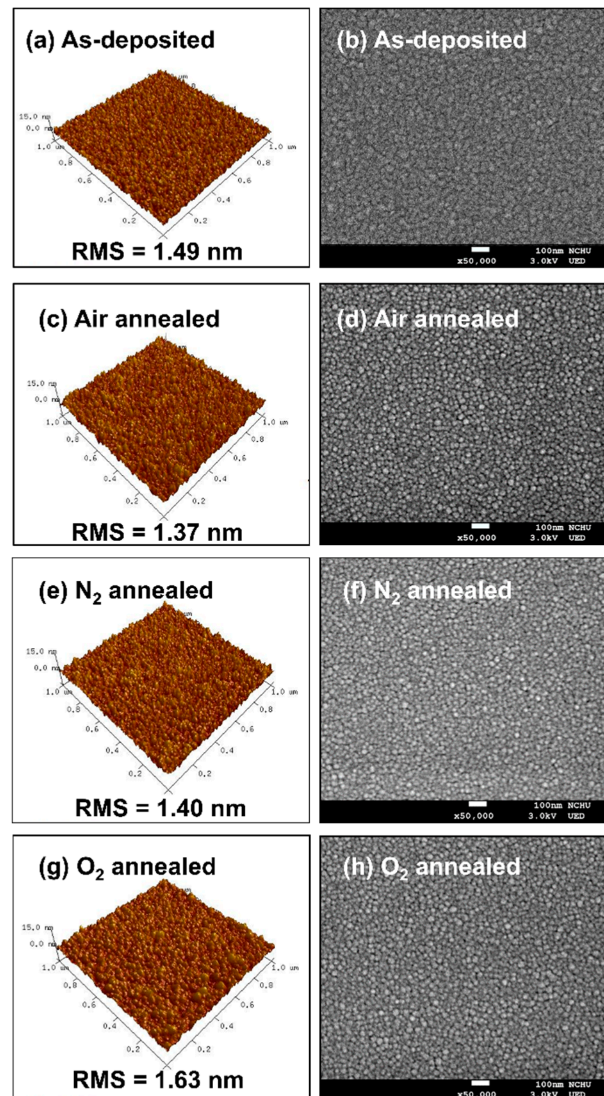

Figure 2. AFM micrographs of (**a**) as-deposited, (**c**) air annealed, (**e**) N_2 annealed, and (**g**) O_2 annealed $ZnGa_2O_4$ films; SEM micrographs of (**b**) as-deposited, (**d**) air annealed, (**f**) N_2 annealed, and (**h**) O_2 annealed $ZnGa_2O_4$ films.

Figure 4a shows the transmittance spectrum of the as-deposited and annealed $ZnGa_2O_4$ films under different annealing ambiences. The average transmittance of the as-deposited and annealed $ZnGa_2O_4$ films was over 82% in the visible range, with a sharp cut-off in the DUV region. The absorption band-edge of the as-deposited film shifted to shorter wavelengths upon thermal annealing, which demonstrated the improvement in the optical characteristics of this film. Figure 4b shows the Tauc plot, which demonstrates the bandgap values for the as-deposited and annealed $ZnGa_2O_4$ films under different ambiences. The transmittances values of these films were taken into consideration to calculate the absorption coefficient α. The optical bandgap of $ZnGa_2O_4$ films was obtained using the following relation:

$$(\alpha h\nu) = A\ (h\nu - E_g)^{1/2} \quad (1)$$

where A, α, hν, and E_g represent the constant, absorption coefficient, energy of the incident photon, and the bandgap energy, respectively. The narrow bandgap of 4.53 eV in the as-deposited $ZnGa_2O_4$ film can be attributed to the existence of defect states (amorphous structure, phase separations between Ga_2O_3 and ZnO), as shown by TEM (see Figure 3b,c). This led the excited electron to migrate to the conduction band with a low photon energy, narrowing the bandgap. Thermal annealing in various ambiences mitigates the defects

(including amorphous nature and oxygen vacancies) that are common in as-deposited $ZnGa_2O_4$ film. As the thermal annealing was employed, the bandgap increased as 4.98, 5.02, and 5.05 eV under oxygen, nitrogen, and air ambiences, respectively, which allowed this material to lie within the DUV region. It is widely known that materials with a bandgap greater than 4.4 eV absorb UV-C radiation while ignoring visible light, making them ideal for use as high-sensitivity DUV PDs.

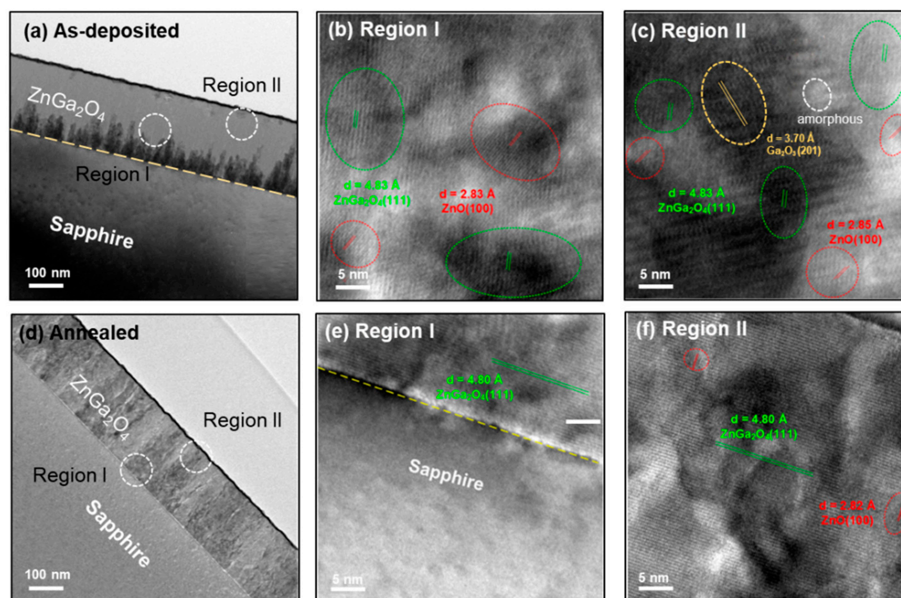

Figure 3. Cross-sectional and HRTEM micrographs of (**a**) as-deposited, (**b**) region I, (**c**) region II of as-deposited $ZnGa_2O_4$ film, (**d**) annealed, (**e**) region I, and (**f**) region II of annealed $ZnGa_2O_4$ film under air ambience.

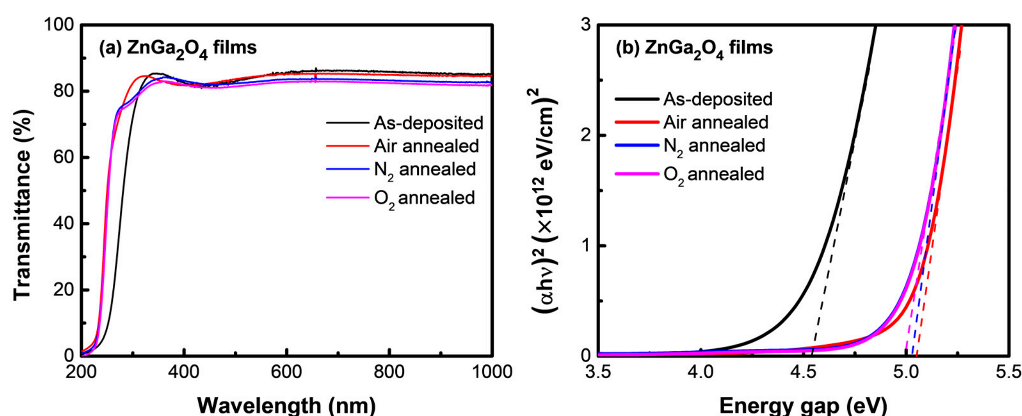

Figure 4. (**a**) Transmittance spectrum and (**b**) Tauc plot of the as-deposited and annealed $ZnGa_2O_4$ films under different annealing ambiences.

Figure 5 shows the O 1s XPS spectra of the as-deposited and annealed $ZnGa_2O_4$ films under different ambiences. In order to define the oxygen vacancies associated with the films, the O 1s XPS spectra of the films were fitted with the Gaussian function and deconvoluted into two peaks named O_I and O_{II}. The O_I peak centered around the lower binding energies of 530–531 eV represents the oxygen deficiency in the films, whereas the O_{II} peak centered at higher binding energies of 531–532 eV represents the oxygen vacancies in the film [27]. The integrated areas of the O_{II} peak of the $ZnGa_2O_4$ films were found to be 43.9, 41.1, 45.3, and 37.6% for as-deposited, air annealed, N_2 annealed, and O_2 annealed ambiences, respectively. The oxygen present in the air ambience can

fill a certain amount of oxygen vacancy. Hence, the area of O_{II} peak was found to be decreased from 43.9 to 41.1% during air annealing, as shown in Figure 5b. The area of the O_{II} peak was found to be higher (45.3%) in an N_2 atmosphere, which can be attributed to the disassociation of oxygen molecules from the films during annealing. This resulted in an increased number of oxygen vacancies, as shown in Figure 5c [25]. By observing the integrated areas of O_{II} peaks from Figure 5a–d, it was found that the O_2-annealed $ZnGa_2O_4$ film had the lowest integrated area of O_{II} peaks (37.6%). It is well-known that an oxygen-rich ambience reduces the number of oxygen vacancies, which weakens the crystalline structure [28]. This phenomenon is in accordance with our XRD results, as shown in Figure 1, where oxygen ambience deteriorated the crystalline structure. Since oxygen vacancies affect the optoelectronic properties of $ZnGa_2O_4$ film, the considerable suppression of oxygen vacancies demonstrates the tunability of the film characteristics depending on the annealing ambiences.

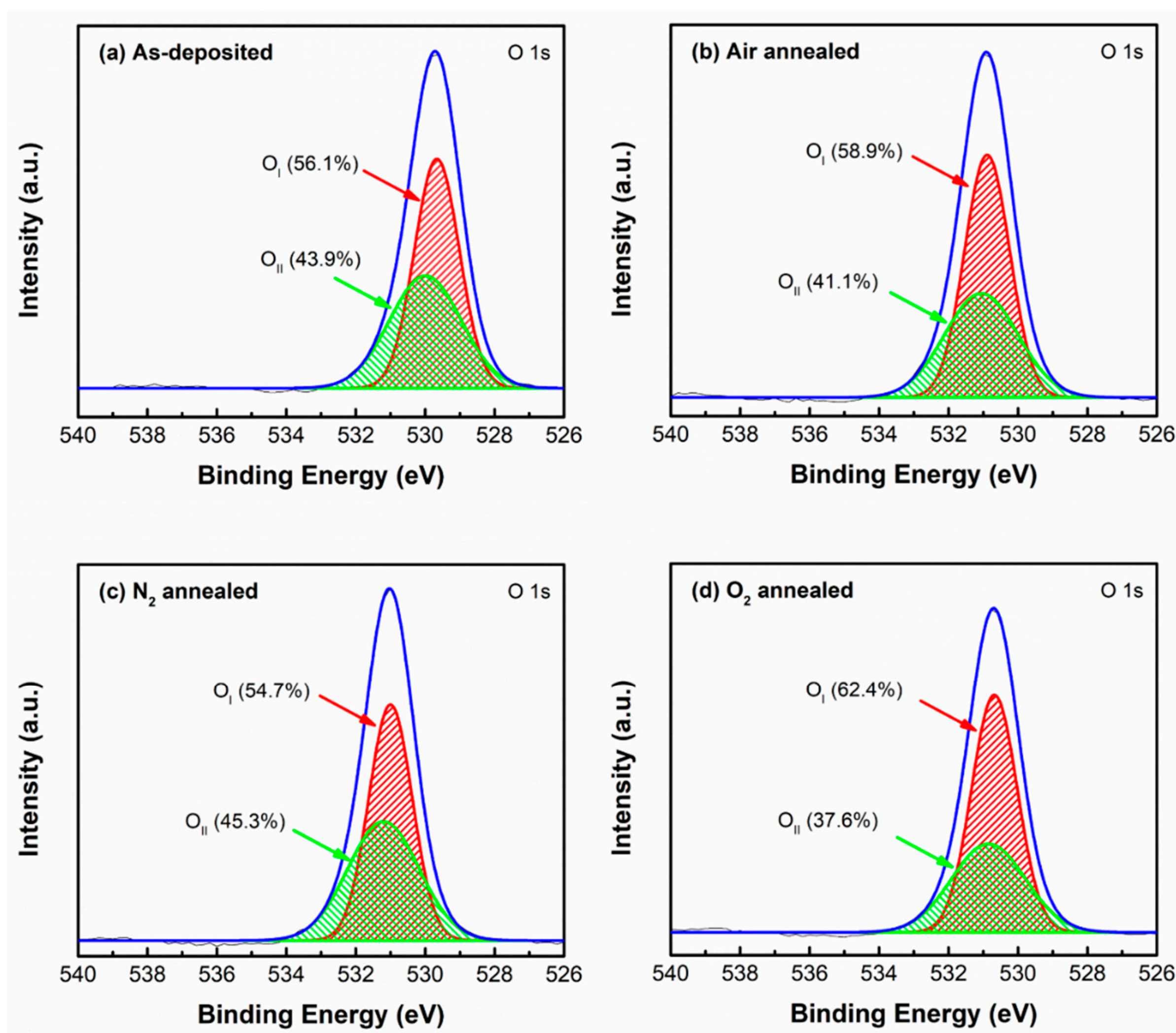

Figure 5. O 1s XPS spectra of (**a**) as-deposited, (**b**) air annealed, (**c**) N_2 annealed, and (**d**) O_2 annealed $ZnGa_2O_4$ films.

Figure 6 shows the I–V characteristics of the as-deposited and annealed $ZnGa_2O_4$ PDs under different annealing ambiences. The as-deposited $ZnGa_2O_4$ PD exhibited the photocurrent and dark current of 5.69×10^{-8} A and 5.77×10^{-12} A, respectively. This photocurrent had decreased from 5.69×10^{-8} to 6.12×10^{-9} A after annealing under oxygen ambience. This decreased photocurrent can be ascribed to the fulfilment of oxygen vacancies during high temperature annealing under oxygen ambience, which oxidized the $ZnGa_2O_4$ films and resulted in the decreased value of photocurrent. Nitrogen ambience

caused the desorption of oxygen atoms from the surface of the films, and created oxygen vacancies, which drastically increased the photocurrent of the as-deposited $ZnGa_2O_4$ PD from 5.69×10^{-8} to 9.64×10^{-6} A. The dark current of as-deposited $ZnGa_2O_4$ PD was also found to be increased from 5.77×10^{-12} to 3.33×10^{-7} A upon annealing this film under nitrogen ambience, which was not desirable for PDs. This high dark current value can be attributed to the high number of inherent defects in the $ZnGa_2O_4$ PDs, such as oxygen vacancies and high surface density states, which can result in trapping states and was responsible for a higher internal gain. As a result, these surface states enhanced the dark current as well as the nonradiative recombination for the $ZnGa_2O_4$ film (annealed under nitrogen ambience). Similar results have been observed by Tsai et al. in their work [29], where surface related defects were the main cause of the large leakage current in their device, which acted as the adsorption site and captured the free electrons in $ZnGa_2O_4$ films. When air ambience was used for annealing, $ZnGa_2O_4$ PD exhibited a photocurrent of 2.02×10^{-7} A, a dark current of 5.35×10^{-12} A, and a I_{ph}/I_{dark} of 3.77×10^4. Annealing $ZnGa_2O_4$ film under air ambience can fill a significant proportion of oxygen vacancies from the oxygen present in the air ambience, which exhibits the enhancement in optoelectronic characteristics of this $ZnGa_2O_4$ film and its potential to employ in DUV PDs.

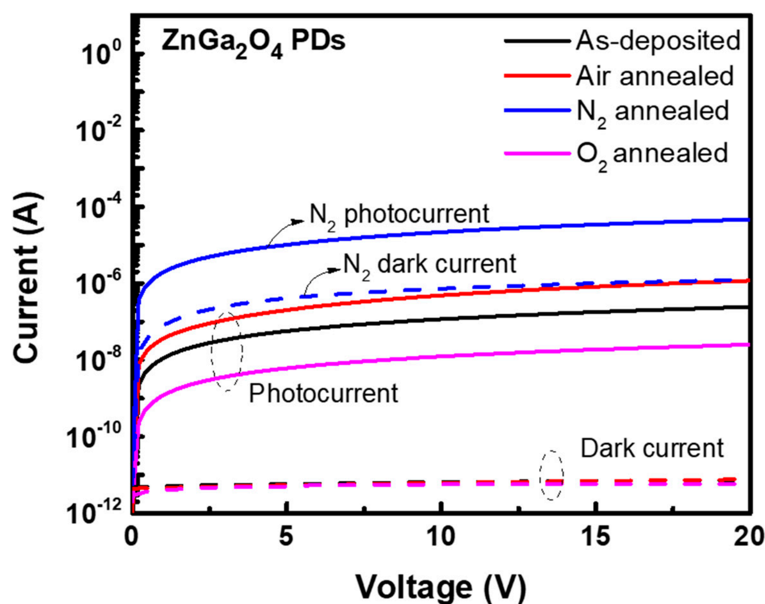

Figure 6. I–V characteristics of the as-deposited and annealed $ZnGa_2O_4$ PDs under different annealing ambiences.

Figure 7 shows the spectral response of the as-deposited and annealed $ZnGa_2O_4$ PDs under different annealing ambiences. The spectral response describes the sensitivity of the photodetector to optical radiation of various wavelengths, which is known as the responsivity of the photodetector. This parameter defines the performance of the photodetector and is represented by the following relation:

$$R = (I_{ph}\text{-}I_{dark})/P_{inc} \tag{2}$$

where I_{ph} is the photocurrent in Ampere (A), I_{dark} is the dark current in Ampere (A), and P_{inc} is the incident optical power in Watt (W). Hence, the responsivity of the photodetector is measured in A/W. As-deposited $ZnGa_2O_4$ PD possessed a responsivity of 0.71 A/W, which decreased to 0.12 A/W upon thermal annealing under oxygen ambience. This decreased responsivity could be due to the fulfilment of oxygen vacancies by oxygen gas, which further decreased the mobility of carriers and exhibited the poor responsivity of the $ZnGa_2O_4$ PD. Annealing under nitrogen ambience drastically increased the responsivity of $ZnGa_2O_4$ PD from 0.71 to 117 A/W. However, N_2 annealed $ZnGa_2O_4$ PD exhibited a

broad spectral response from the DUV region to the visible region, which was not suitable for the DUV PDs. Annealing under nitrogen ambience reduced the oxygen concentration from the film and generated oxygen vacancy defects and surface density states. These defects led to the creation of deep-trapping centers, which increased the photocurrent as well as the dark current and enhanced the internal gain for $ZnGa_2O_4$ PD [29]. Zheng et al. and Han et al. reported that the high responsivity of $Mg_{0.46}Zn_{0.54}O$ and $Mg_{0.52}Zn_{0.48}O$ films-based photodetectors is due to the long lifetime of photo-ionized holes, which were found to be trapped at the deep level. This measurement was precisely taken by using deep-level spectral measurement system in their works [30,31]. The trap states of holes include interface states between semiconductor and electrode, surface states, and deep level defects. These trap states were found responsible for this long lifetime phenomenon. It is clear that the photoresponse characteristics of $ZnGa_2O_4$ PDs could represent variations due to various oxygen vacancy related defects, which can be suppressed by the adaptation of air ambience. A large amount of oxygen molecules or atoms in the air ambience will diffuse into the samples and fill the significant number of oxygen vacancies, resulting in low surface density states [32]. Annealing under air ambience exhibited both a significant enhancement in the photocurrent and reduction in the dark current by providing adequate energy to compensate the oxygen vacancy related defects. Hence, the responsivity of 2.53 A/W at the given bias of 5 V under the incident optical light of 240 nm was obtained for $ZnGa_2O_4$ PD under air ambience. The performance of our fabricated device is compared with that of the previously reported $ZnGa_2O_4$ PDs in Table 1.

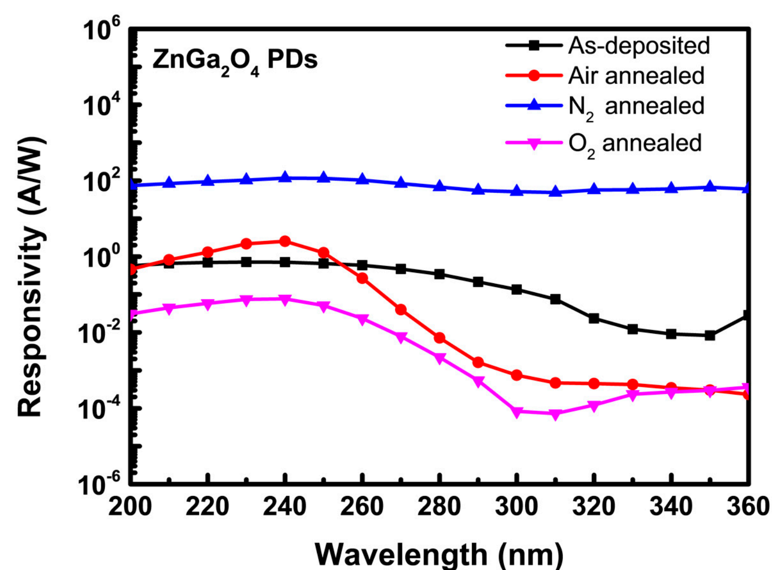

Figure 7. Spectral response of as-deposited and annealed $ZnGa_2O_4$ PDs under different annealing ambiences.

Table 1. Comparison of some key performance of our $ZnGa_2O_4$ PD with other previously reported $ZnGa_2O_4$ PDs.

Material	Growth Method	I_{dark} (A)	I_{ph} (A)	R (A/W)	Bias Voltage and λ_{peak}	Reference
$ZnGa_2O_4$	MOCVD	$\sim 10^{-14}$	2.93×10^{-6}	0.203	10 V, 260 nm	[33]
$ZnGa_2O_4$	MOCVD	0.86×10^{-12}	4.04×10^{-8}	0.46	10 V, 230 nm	[34]
$ZnGa_2O_4$	Sputter	2.70×10^{-11}	-	-	2 V, 255 nm	[35]
$ZnGa_2O_4$	Sputter	5.35×10^{-12}	2.02×10^{-7}	2.53	5 V, 240 nm	This work

Figure 8 shows the rise time and fall time for the as-deposited and annealed $ZnGa_2O_4$ PDs under different annealing ambiences. Rise time is the time that the PD takes to change its response from 10% to 90% of the maximum photocurrent with the illumination of light. Fall

time is the time that the PD takes to change its response from 90% to 10% of the maximum photocurrent without the illumination of light. These two characteristics (rise time and fall time) represent the response time of a photodetector. $ZnGa_2O_4$ PD annealed under air ambience possesses a higher rise time of 4.55 s but a lesser fall time of 0.19 s than other PDs (as-deposited, annealed $ZnGa_2O_4$ PDs under nitrogen and oxygen ambiences), which could be due to the indirect bandgap properties of the spinel-cubic $ZnGa_2O_4$ structure [36]. The high rise time for the $ZnGa_2O_4$ PD annealed under air ambience could be attributed to the excitation of photogenerated carriers, which reached higher energy states above the conduction band. These excited photogenerated carriers then reverted to the conduction band by releasing energy and resulted in a high rise time. Despite the fact that the response time of $ZnGa_2O_4$ PDs annealed in air ambience is higher than that of other $ZnGa_2O_4$ PDs annealed under other ambiences, the responsivity associated with this air annealed $ZnGa_2O_4$ PD is found to be considerable for use in DUV PDs.

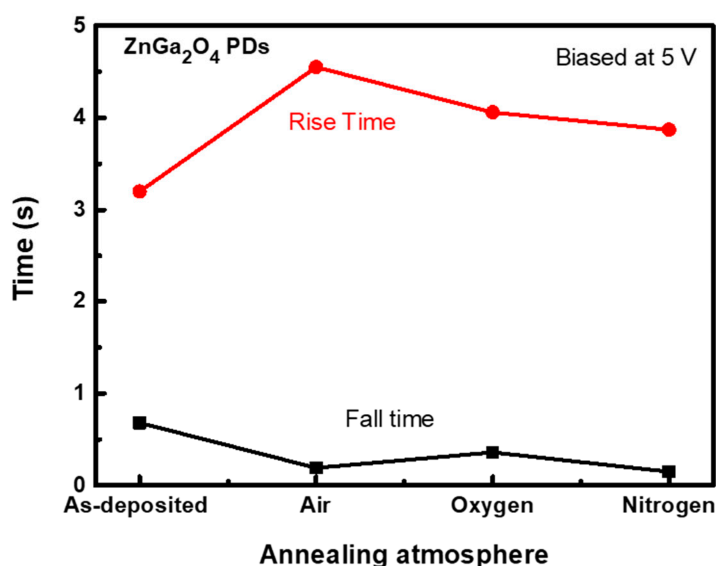

Figure 8. Time response of as-deposited and annealed $ZnGa_2O_4$ PDs under different annealing ambiences.

4. Conclusions

We have successfully deposited $ZnGa_2O_4$ films on sapphire substrates using RF magnetron sputtering, as well as studied the effects of thermal annealing in various ambiences (such as air, nitrogen, and oxygen) on the material and photodetector characteristics of $ZnGa_2O_4$ films. Investigations using XRD, AFM, SEM, TEM, N&K analyzer, and DUV measurements revealed that the microstructural and optoelectronic characteristics of $ZnGa_2O_4$ films were enhanced under air ambience and affected under nitrogen and oxygen ambiences. These results were verified by comparatively analyzing the chemical states of oxygen on the surface of the $ZnGa_2O_4$ films before and after annealing in different ambiences using XPS. The X-ray diffraction patterns of the annealed $ZnGa_2O_4$ films exhibited crystalline structures with (111) crystallographic planes. The as-deposited $ZnGa_2O_4$ film possessed amorphous regions and phase separations between Ga_2O_3 and ZnO, which were found to be suppressed after annealing under air ambience. The TEM micrographs revealed that $ZnGa_2O_4$ film annealed under air ambience possessed a quasi-single-crystalline structure. The average transmittance of 82% in the visible region and wide bandgap of 5.05 eV were observed for this $ZnGa_2O_4$ film. The metal-semiconductor-metal PD fabricated by employing this air annealed $ZnGa_2O_4$ film exhibited the high responsivity of 2.53 A/W at the bias of 5 V under the incident light of 240 nm. Besides this, $ZnGa_2O_4$ PD had a rise time of 4.55 s, a fall time of 0.19 s, and a photo/dark current ratio of ~10^4 order. These results indicate that quasi-single-crystalline $ZnGa_2O_4$ films have a high potential to employ in DUV PDs.

Author Contributions: Writing—original draft, A.K.S.; methodology, A.K.S. and S.-Y.H.; validation, A.K.S., P.-W.C.; data curation, A.K.S. and S.-Y.H.; writing—review and editing, A.K.S., P.-W.C., J.-L.C. and D.-S.W.; Conceptualization, supervision, project administration, and funding acquisition, D.-S.W. All authors have read and agreed to the published version of the manuscript.

Funding: This work was supported by the Ministry of Science and Technology (Taiwan, R.O.C.) under Grant Nos. 108-2221-E-005-028-MY3 and 109-2811-E-005-508-MY2. The authors also wish to express their sincere gratitude for the financial support from the "Innovation and Development Center of Sustainable Agriculture" from The Featured Areas Research Center Program within the framework of the Higher Education Sprout Project by the Ministry of Education (MOE) in Taiwan.

Institutional Review Board Statement: Not Applicable.

Informed Consent Statement: Not Applicable.

Data Availability Statement: The data that support the findings of this study are available from the corresponding author upon reasonable request.

Acknowledgments: The authors express their sincere gratitude for the technical support from the Advanced Industry Technology Centre of National Chung Hsing University, Taiwan. The authors acknowledge the "Instrument Centre of National Chung Hsing University" for SEM, TEM, and AFM, and XPS measurements.

Conflicts of Interest: The authors declare no conflict of interest.

References

1. Liao, M.; Koide, Y. High-performance metal-semiconductor-metal deep-ultraviolet photodetectors based on homoepitaxial diamond thin film. *Appl. Phys. Lett.* **2006**, *89*, 3–6. [CrossRef]
2. Han, D.; Liu, K.; Hou, Q.; Chen, X.; Yang, J.; Li, B.; Zhang, Z.; Liu, L.; Shen, D. Self-powered solar-blind $ZnGa_2O_4$ UV photodetector with ultra-fast response speed. *Sens. Actuators A Phys.* **2020**, *315*, 112354. [CrossRef]
3. Fan, M.M.; Liu, K.W.; Chen, X.; Wang, X.; Zhang, Z.Z.; Li, B.H.; Shen, D.Z. Mechanism of Excellent Photoelectric Characteristics in Mixed-Phase ZnMgO Ultraviolet Photodetectors with Single Cutoff Wavelength. *ACS Appl. Mater. Interfaces* **2015**, *7*, 20600–20606. [CrossRef] [PubMed]
4. Sang, L.; Liao, M.; Sumiya, M. A comprehensive review of semiconductor ultraviolet photodetectors: From thin film to one-dimensional nanostructures. *Sensors* **2013**, *13*, 10482–10518. [CrossRef] [PubMed]
5. Han, N.; Chen, D.; Pang, Y.; Han, Z.; Xia, Y.; Jiao, X. Structural regulation of $ZnGa_2O_4$ nanocubes for achieving high capacity and stable rate capability as an anode material of lithium ion batteries. *Electrochim. Acta* **2017**, *235*, 295–303. [CrossRef]
6. Si, T.; Zhu, Q.; Zhang, T.; Sun, X.; Li, J.-G. Co-doping Mn^{2+}/Cr^{3+} in $ZnGa_2O_4$ to fabricate chameleon-like phosphors for multi-mode dynamic anti-counterfeiting. *Chem. Eng. J.* **2021**, *426*, 131744. [CrossRef]
7. Garcia, C.R.; Oliva, J.; Diaz-Torres, L.A.; Montes, E.; Hirata, G.; Bernal-Alvarado, J.; Gomez-Solis, C. Controlling the white phosphorescence $ZnGa_2O_4$ phosphors by surface defects. *Ceram. Int.* **2019**, *45*, 4972–4979. [CrossRef]
8. Hsieh, I.J.; Chu, K.T.; Yu, C.F.; Feng, M.S. Cathodoluminescent characteristics of $ZnGa_2O_4$ phosphor grown by radio frequency magnetron sputtering. *J. Appl. Phys.* **1994**, *76*, 3735–3739. [CrossRef]
9. Lee, Y.E.; Norton, D.P.; Budai, J.D.; Wei, Y. Enhanced ultraviolet photoconductivity in semiconducting $ZnGa_2O_4$ thin films. *J. Appl. Phys.* **2001**, *90*, 3863–3866. [CrossRef]
10. Li, H.; Yuan, S.H.; Huang, T.M.; Chen, H.J.; Lu, F.H.; Zhang, S.; Wuu, D.S. Impact of thermal-induced sapphire substrate erosion on material and photodetector characteristics of sputtered Ga_2O_3 films. *J. Alloys Compd.* **2020**, *823*, 153755. [CrossRef]
11. Chen, M.I.; Singh, A.K.; Chiang, J.L.; Horng, R.H.; Wuu, D.S. Zinc gallium oxide—A review from synthesis to applications. *Nanomaterials* **2020**, *10*, 2208. [CrossRef]
12. Chi, Z.; Tarntair, F.-G.; Frégnaux, M.; Wu, W.-Y.; Sartel, C.; Madaci, I.; Chapon, P.; Sallet, V.; Dumont, Y.; Pérez-Tomás, A.; et al. Bipolar self-doping in ultra-wide bandgap spinel $ZnGa_2O_4$. *Mater. Today Phys.* **2021**, *20*, 100466. [CrossRef]
13. Chikoidze, E.; Sartel, C.; Madaci, I.; Mohamed, H.; Vilar, C.; Ballesteros, B.; Belarre, F.; Del Corro, E.; Vales-Castro, P.; Sauthier, G.; et al. P-Type Ultrawide-Band-Gap Spinel $ZnGa_2O_4$: New Perspectives for Energy Electronics. *Cryst. Growth Des.* **2020**, *20*, 2535–2546. [CrossRef]
14. Dong, L.; Jia, R.; Xin, B.; Zhang, Y. Effects of post-annealing temperature and oxygen concentration during sputtering on the structural and optical properties of β-Ga_2O_3 films. *J. Vac. Sci. Technol. A Vac. Surf. Film.* **2016**, *34*, 60602. [CrossRef]
15. Jang, Y.; Hong, S.; Seo, J.; Cho, H.; Char, K.; Galazka, Z. Thin film transistors based on ultra-wide bandgap spinel $ZnGa_2O_4$. *Appl. Phys. Lett.* **2020**, *116*, 3–8. [CrossRef]
16. Satya Kamal, C.; Boddu, S.; Vishwanadh, B.; Rao, K.R.; Sudarsan, V.; Vatsa, R.K. Blue luminescence from $ZnGa_2O_4$: Effect of lattice distortion and particle size. *J. Lumin.* **2017**, *188*, 429–435. [CrossRef]
17. Lou, Z.; Li, L.; Shen, G. High-performance rigid and flexible ultraviolet photodetectors with single-crystalline $ZnGa_2O_4$ nanowires. *Nano Res.* **2015**, *8*, 2162–2169. [CrossRef]

18. Bae, S.Y.; Lee, J.; Jung, H.; Park, J.; Ahn, J.P. Helical structure of single-crystalline $ZnGa_2O_4$ nanowires. *J. Am. Chem. Soc.* **2005**, *127*, 10802–10803. [CrossRef] [PubMed]
19. Lee, C.S.; Cuong, H.B.; Jeong, S.H.; Lee, B.T. Comparative study of group-II alloying effects on physical property of ZnGaO transparent conductive films prepared by RF magnetron sputtering. *J. Alloys Compd.* **2015**, *645*, 322–327. [CrossRef]
20. Kumar Singh, A.; Chen, P.-W.; Wuu, D.-S. Growth and characterization of co-sputtered Al-doped $ZnGa_2O_4$ films for enhancing deep-ultraviolet photoresponse. *Appl. Surf. Sci.* **2021**, *566*, 150714. [CrossRef]
21. Shi, Q.; Wang, C.; Zhang, D.; Li, S.; Zhang, L.; Wang, W.; Zhang, J. Luminescence of Cr^{3+}-doped $ZnGa_2O_4$ thin films deposited by pulsed laser ablation. *Thin Solid Films* **2012**, *520*, 6845–6849. [CrossRef]
22. Lin, X.; Chen, D.; Niu, W.; Huang, C.Y.; Horng, R.H.; Cheng, L.C.; Talwar, D.N.; Lin, H.H.; Lee, J.F.; Feng, Z.C.; et al. Evolution of the local structure and crystal phase for thin ZnGaO films grown by metal organic chemical vapor deposition. *J. Cryst. Growth* **2019**, *520*, 89–95. [CrossRef]
23. Oshima, T.; Niwa, M.; Mukai, A.; Nagami, T.; Suyama, T.; Ohtomo, A. Epitaxial growth of wide-band-gap $ZnGa_2O_4$ films by mist chemical vapor deposition. *J. Cryst. Growth* **2014**, *386*, 190–193. [CrossRef]
24. Sun, R.; Zhang, H.Y.; Wang, G.G.; Han, J.C.; Wang, X.Z.; Kuang, X.P.; Cui, L.; Jin, L.; Tian, J.L. Influence of annealing atmosphere on the structure, morphology and transmittance of N-incorporated Ga_2O_3 films. *Superlattices Microstruct.* **2013**, *60*, 257–262. [CrossRef]
25. Tien, C.H.; Hsiao, B.W.; Chen, C.M.; Chen, M.I.; Chiang, J.L.; Wuu, D.S. Nitrogen and oxygen annealing effects on properties of aluminum-gallium oxide films grown by pulsed laser deposition. *Ceram. Int.* **2020**, *46*, 24147–24154. [CrossRef]
26. Aswal, D.K.; Muthe, K.P.; Tawde, S.; Chodhury, S.; Bagkar, N.; Singh, A.; Gupta, S.K.; Yakhmi, J.V. XPS and AFM investigations of annealing induced surface modifications of MgO single crystals. *J. Cryst. Growth* **2002**, *236*, 661–666. [CrossRef]
27. Cheng, L.-C.; Wu, M.-R.; Huang, C.-Y.; Juang, T.-K.; Liu, P.-L.; Horng, R.-H. Effect of Defects on the Properties of $ZnGa_2O_4$ Thin-Film Transistors. *ACS Appl. Electron. Mater.* **2019**, *1*, 253–259. [CrossRef]
28. Huang, C.Y.; Horng, R.H.; Wuu, D.S.; Tu, L.W.; Kao, H.S. Thermal annealing effect on material characterizations of β-Ga_2O_3 epilayer grown by metal organic chemical vapor deposition. *Appl. Phys. Lett.* **2013**, *102*, 100–103. [CrossRef]
29. Tsai, S.H.; Basu, S.; Huang, C.Y.; Hsu, L.C.; Lin, Y.G.; Horng, R.H. Deep-Ultraviolet Photodetectors Based on Epitaxial $ZnGa_2O_4$ Thin Films. *Sci. Rep.* **2018**, *8*, 14056. [CrossRef]
30. Zheng, Q.; Huang, F.; Huang, J.; Hu, Q.; Chen, D.; Ding, K. High-Responsivity Solar-Blind Photodetector Based on Mg_0 46Zn0.54O Thin Film. *IEEE Electron. Device Lett.* **2012**, *33*, 1033–1035. [CrossRef]
31. Han, S.; Zhang, Z.; Zhang, J.; Wang, L.; Zheng, J.; Zhao, H.; Zhang, Y.; Jiang, M.; Wang, S.; Zhao, D.; et al. Photoconductive gain in solar-blind ultraviolet photodetector based on $Mg_{0.52}Zn_{0.48}O$ thin film. *Appl. Phys. Lett.* **2011**, *99*, 242105. [CrossRef]
32. Sundara Venkatesh, P.; Balakumar, S.; Jeganathan, K. Post-annealing effects on the structural and optical properties of vertically aligned undoped ZnO nanorods grown by radio frequency magnetron sputtering. *RSC Adv.* **2014**, *4*, 5030–5035. [CrossRef]
33. Huang, W.-L.; Li, C.-H.; Chang, S.-P.; Chang, S.-J. The Effect of Oxygen Partial Pressure and Annealing Process on the Characteristics of $ZnGa_2O_4$ MSM UV Photodetector. *ECS J. Solid State Sci. Technol.* **2019**, *8*, Q3213–Q3216. [CrossRef]
34. Tsai, S.H.; Shen, Y.C.; Huang, C.Y.; Horng, R.H. Deep-ultraviolet Schottky photodetectors with high deep-ultraviolet/visible rejection based on a $ZnGa_2O_4$ thin film. *Appl. Surf. Sci.* **2019**, *496*, 143670. [CrossRef]
35. Lin, W.; Zhang, D.; Liu, S.; Li, Y.; Zheng, W.; Huang, F. $ZnGa_2O_4$ deep-ultraviolet photodetector based on Si substrate. *Mater. Lett.* **2021**, *283*, 128805. [CrossRef]
36. Chen, P.W.; Huang, S.Y.; Yuan, S.H.; Chen, Y.A.; Hsiao, P.W.; Wuu, D.S. Quasi-Single-Crystalline $ZnGa_2O_4$ Films via Solid Phase Epitaxy for Enhancing Deep-Ultraviolet Photoresponse. *Adv. Mater. Interfaces* **2019**, *6*, 1901075. [CrossRef]